Mathematical Model of a Damped Rate-of-Climb Indicator

D. Adler*
Technion—Israel Institute of Technology, Haifa, Israel

A damped rate of climb indicator is mathematically modeled. The resulting set of simultaneous equations is solved numerically, and the solution is compared to experiments. Agreement of the calculations and experimental results is good. Thus the mathematical model can be used for numerical simulation, optimization, and design of rate of climb indicators.

Nomenclature

a = constant in Eq. (3)
b = constant in Eq. (3)
C_T = constant defined in Eqs. (12) and (13)
c_1 to c_{15} = auxiliary functions defined in Eqs. (18)-(23) and (34)-(42)
D = diameter of the diaphragm (see Fig. 3)
E = modulus of elasticity
H = corrugations height of the diaphragm (see Fig. 3)
h = altitude
M = stiffness coefficient of the diaphragm in its linear region [defined in Eq. (5)]
m = mass contained in the compartments of the rate of climb indicator
p = static pressure
R = gas constant
S = diaphragm thickness (see Fig. 3)
T = static temperature
t = time
V = volume of the compartments of the rate of climb meter
V_B = total volume of the compartments ($V_B = V_1 + V_2$)
v = velocity
x = displacement of the diaphragm (instrument indication)
α = ratio of compartment volumes ($\alpha = V_1/V_2$)
β = $(H/S)^2$
γ = shape function of the diaphragm (constant in the present case) defined as the ratio between the volume under the deflected diaphragm and the volume of a cylinder of diameter D and height x
κ = specific heats ratio
μ = Poisson's ratio
ν = kinematic viscosity
ξ = pressure loss coefficient, defined in Eqs. (8, 9, 24, and 25)
ρ = density

Subscripts

0 = initial condition
1 = referring to compartment 1
2 = referring to compartment 2

Introduction

THE rate of climb indicator was originally proposed in 1910 by Bestelmeyer[1] as an undamped instrument (Fig. 1). Modern rate of climb indicators, however, are equipped with a damping capillary (Fig. 2). Theoretical studies of undamped rate of climb indicators were carried out by a number of investigators.[2-9] During the Second World War, Takeda[10] developed an improved mathematical model of a damped rate of climb indicator. Takeda's model is based on the continuity equation and the equation of state only; the energy equation is not satisfied in his theory. Like Bestelmeyer and many of the other early investigators, Takeda neglects terms including dT_1/dt, dT_2/dt, etc. This may not be justified in instruments with small values of α at high rates of altitude variation.

In the present study a mathematical model of a damped rate of climb indicator is developed which satisfies also the energy equation, and in which no temperature terms are neglected. This leads to a model which represents temperature effects in a more realistic form. Using the energy equation it is shown that because of the basic difference between the energy transfer in the instrument during descent and climb, the mathematical description of the two processes is not identical. The present model also includes directly the influence of the geometry and material of the diaphragm.

Mathematical Model

The rate of climb indicator is given a schematic form for the mathematical treatment (Fig. 2). Here, each of the compartments has a single connection with the atmosphere, but this does not restrict the generality of the model as any number of parallel flow passages can be replaced by an equivalent single flow passage.

The unknown quantities during altitude change are the conditions, the volume, and the mass in each of the compartments, namely, p_1, ρ_1, T_1, V_1, m_1, p_2, ρ_2, T_2, V_2, m_2,

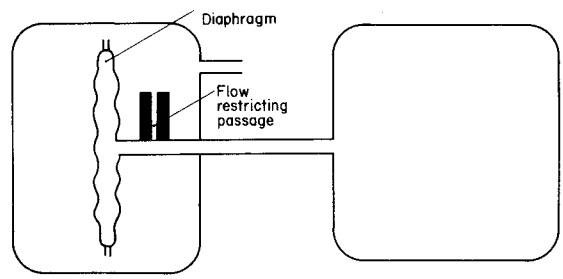

Fig. 1 Schematic description of an undamped rate of climb indicator.

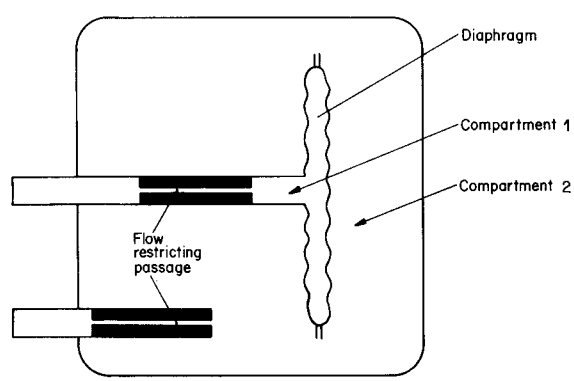

Fig. 2 Schematic description of a damped rate of climb indicator.

Received June 6, 1973; revision received May 8, 1974. This work was carried out with the valuable help of E. Eshkoli who did the computer work and operated the test rig.

Index categories: Aircraft Subsystem Design; Aircraft Navigation, Communication, and Traffic Control.

*Senior Lecturer, Department of Mechanical Engineering.

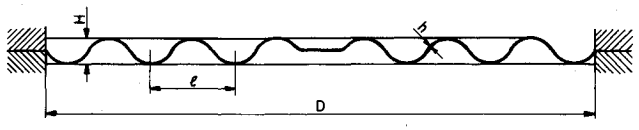

Fig. 3 Corrugated diaphragm.

and the displacement of the diaphragm x. These eleven quantities depend on the time t. Known are the instrument constants, V_B, the total volume of both compartments which is constant; α, the ratio between V_1 and V_2 when $x = 0$; M, the stiffness coefficient of the diaphragm; γ, the shape constant of the diaphragm; all the dimensions of the diaphragm (see Fig. 3); and ξ_1 and ξ_2, the functions describing the pressure loss coefficients of the flow passages which are not constants and depend on the density and the viscosity of the through flowing air. The atmospheric conditions $p_0(h)$ and $T_0(h)$ and the altitude variation $h(t)$ are also known. Therefore, the atmospheric conditions can be written as functions of time: $p_0[h(t)]$ and $T_0[h(t)]$. Eleven simultaneous equations for the eleven unknown quantities are written and solved. These equations include all the instrument constants mentioned.

The displacement of the diaphragm is governed by the change of volume in the two interdependent compartments (which are charged during descent and evacuated during climb), and by the dynamic behavior of the diaphragm. It is assumed that because of the small mass and displacements inertia effects of the diaphragm can be neglected. Hysteresis effects of the diaphragm can be held as low as 0.01% of the diaphragm diameter,[11] and are therefore also neglected in this study. These assumptions are varified experimentally. The charging process of the compartments during descent differs physically, and therefore also mathematically, from the evacuation during climb. During descent the air in the compartments is compressed and mixed with the external inflowing air. During climb, on the other hand, only expansion of the air takes place in the compartments. This difference is not significant when both compartments are large, but when one of the compartments is small like the indicator of Fig. 2, the difference between descent and climb must be taken into account.

A. Climb

The climb model satisfies the basic equations which describe the coupled evacuation of the two compartments. These equations must be solved simultaneously.

The equation of state for each of the two compartments is:

$$p_1 = \rho_1 R T_1 \tag{1}$$

$$p_2 = \rho_2 R T_2 \tag{2}$$

The displacement equation of the diaphragm is the condition which couples both compartments. It is written here for a shallow double sinusoidal corrugated diaphragm[12] as in Fig. 3. The influence of the connection in the center is neglected. (Information on this and displacement equations of other types of diaphragms can be found in Ref. 12.)

$$p_1 - p_2 = \frac{16E}{D^4}\left(\frac{as^3}{3}x + \frac{bs}{8}x^3\right) \tag{3}$$

where

$$a = \frac{2\left[3 + \left(\frac{3}{2}\beta + 1\right)^{1/2}\right]\left[1 + \left(\frac{3}{2}\beta + 1\right)^{1/2}\right]}{3\left[1 - \mu^2/\left(\frac{3}{2}\beta + 1\right)\right]}$$

$$b = \frac{32}{\frac{3}{2}\beta - 8} \times \left\{\frac{1}{6} - \frac{3 - \mu}{\left[\left(\frac{3}{2}\beta + 1\right)^{1/2} - \mu\right]\left[\left(\frac{3}{2}\beta + 1\right)^{1/2} + 3\right]}\right\}$$

For corrugated diaphragms $b < a$ so that the second term in the brackets of Eq. (3) can be neglected for small displacements. Let us consider for example, a diaphragm with: $S = 0.22$mm, $H = 0.75$mm, $D = 50$mm, and $E = 1 \times 10^6$kg/cm^2. In this case we have

$$p_2 - p_1 = 0.353x + 0.0175x^3$$

for a relative large displacement of $x = 0.5$mm the contribution of the second right-hand side term is about 0.8%. This fact justifies the assumption that the diaphragm is linear in its present range of application and can be described by:

$$x = D^4(p_2 - p_1)/8ES^3a \tag{4}$$

Equation (4) defines the stiffness coefficients of the diaphragm M,

$$M = D^4/8ES^3a \tag{5}$$

The displacement x is positive for climb, where $p_2 > p_1$, if $\xi_2 > \xi_1$.

The mass of air contained in each of the compartments at any instant is

$$m_1 = \left(\frac{\alpha V_B}{1 + \alpha} - \frac{\pi}{4}D^2x\gamma\right)\rho_1 \tag{6}$$

$$m_2 = \left(\frac{V_B}{1 + \alpha} + \frac{\pi}{4}D^2x\gamma\right)\rho_2 \tag{7}$$

where γ, the shape function, is dependent on x. It is defined as the ratio between the volume under the displaced diaphragm and the volume of a cylinder of diameter D and height x. When the displacements x are small, as in the present case, γ can be considered constant.

The pressure losses through the flow restrictions connecting the compartments to the atmosphere are:

$$p_1 - p_0 = \frac{\rho_1}{2}v_1^2\xi_1 \tag{8}$$

$$p_2 - p_0 = \frac{\rho_2}{2}v_2^2\xi_2 \tag{9}$$

These two equations actually define ξ, the pressure loss coefficients. When p_1, p_2, and p_0 are measured in the compartments and in the atmosphere, respectively, then the pressure loss includes all losses involved, including entry and exit losses of the flow passages. These passages can be either long, small diameter tubes, porous plugs, or any other flow resisting passage. The pressure loss coefficients can be calculated for tubes or be evaluated experimentally based on Eqs. (8) and (9) in other cases.

Generally the pressure loss coefficients are not constant and depend on the density and viscosity inside the flow passages. But as both these quantities depend on the temperature and the pressure, we can write for the case of climb (where the compartments are evacuated),

$$\xi_1 = \xi_1(p_1, T_1) \text{ and } \xi_2 = \xi_2(p_2, T_2).$$

These two functions are incorporated in the climb model.

Mass conservation leads to the following two equations:

$$dm_1/dt = -\rho_1 \frac{\pi}{4} d_1^2 v_1 \tag{10}$$

$$dm_2/dt = -\rho_2 \frac{\pi}{4} d_2^2 v_2 \tag{11}$$

where d_1 and d_2 are arbitrary characteristic diameters of the flow passages at the section at which the velocities v_1 and v_2 are measured for the determination of the pressure loss coefficients.

Energy conservation gives:

$$T_1 p_1^{(1-\kappa)/\kappa} = T_{10} p_{10}^{(1-\kappa)/\kappa} = C_{T1} \tag{12}$$

$$T_2 p_2^{(1-\kappa)/\kappa} = T_{20} p_{20}^{(1-\kappa)/\kappa} = C_{T2} \tag{13}$$

where adiabatic expansion inside the compartments is assumed. Second index zero in these equations denotes a condition at the beginning of the climb.

These equations, together with $p_0 = f[h(t)]$, describe the climb process completely and allow the calculation of the eleven unknown time dependent quantities. Of these, $x(t)$ is the quantity which is of direct interest in this problem. After some algebraic manipulations the eleven equations of the climb process are transformed into the following two equations:

$$\begin{aligned} &-\frac{\pi d_1^2}{4RC_{T1}}\left(p_2 - \frac{x}{M}\right)^{1/\kappa}\left[\frac{2RC_{T1}(p_2 - x/M - p_0)}{(p_2 - x/M)^{1/\kappa}\xi_1}\right]^{1/2} \\ &= \frac{\alpha V_B}{(1+\alpha)\kappa RC_{T1}}(p_2 - x/M)^{(1-\kappa)/\kappa}\left(\frac{dp_2}{dt} - \frac{dx}{dt}\frac{1}{M}\right) \\ &\quad - \frac{\pi D^2 \gamma}{4}\left[\frac{x(p_2 - x/M)^{(1-\kappa)/\kappa}}{\kappa RC_{T1}}\left(\frac{dp_2}{dt} - \frac{dx}{dt}\frac{1}{M}\right)\right. \\ &\quad \left. + \frac{(p_2 - x/M)^{1/\kappa}}{RC_{T1}}\frac{dx}{dt}\right] \end{aligned} \tag{14}$$

$$\begin{aligned} &-\frac{\pi d_2^2}{4RC_{T2}} p_2^{1/\kappa}\left[\frac{2RC_{T2}(p_2 - p_0)}{p_2^{1/\kappa}\xi_2}\right]^{1/2} \\ &= \frac{V_B}{(1+\alpha)\kappa RC_{T2}} p_2^{(1-\kappa)/\kappa}\frac{dp_2}{dt} + \frac{\pi D^2\gamma}{4}\left[\frac{x p_2^{(1-\kappa)/\kappa}}{\kappa RC_{T2}}\frac{dp_2}{dt}\right. \\ &\quad \left. + \frac{p_2^{1/\kappa}}{RC_{T2}}\frac{dx}{dt}\right] \end{aligned} \tag{15}$$

Equations (14) and (15) include three time-dependent quantities: $x(t)$, $p_2(t)$, and $p_0(t)$. p_2 is the pressure in one of the compartments, it is an auxiliary function required for the solution and is of no special interest. p_0 is the atmospheric pressure, considered given in the present formulation, and x is the indication which is to be predicted by the mathematical model. Equations (14) and (15) are subject to appropriate initial conditions and can only be solved numerically. Being an initial value problem, the set of equations can be solved by a forward integration method. Here a four point Runge-Kutta method is used. For this purpose the equations must be rearranged and given in a new form, where the symbols c_i denote various combinations of three unknown quantities. They are defined in Eqs. (18–23) as follows.

$$\frac{dx}{dt} = \frac{c_1 - c_2 c_4/c_3}{c_5 + c_6 c_2/c_3} \tag{16}$$

$$\frac{dp_2}{dt} = \frac{-c_4 - c_6(dx/dt)}{c_3} \tag{17}$$

where

$$c_1 = \frac{\pi d_1^2}{4RC_{T1}}\left[\frac{2RC_{T1}(p_2 - x/M - p_0)}{(p_2 - x/M)^{1/\kappa}\xi_1}\right]^{1/2}(p_2 - x/M)^{1/\kappa} \tag{18}$$

$$c_2 = \frac{(p_2 - x/M)^{(1-\kappa)/\kappa}}{\kappa RC_{T1}}\left(\frac{\alpha V_B}{1+\alpha} - \frac{\pi D^2\gamma}{4}x\right) \tag{19}$$

$$c_3 = \frac{p_2^{(1-\kappa)/\kappa}}{\kappa RC_{T2}}\left(\frac{V_B}{1+\alpha} + \frac{\pi D^2\gamma}{4}x\right) \tag{20}$$

$$c_4 = \frac{\pi d_2^2}{4RC_{T2}}\left[\frac{2RC_{T2}(p_2 - p_0)}{p_2^{1/\kappa}\xi_2}\right]^{1/2} p_2^{1/\kappa} \tag{21}$$

$$\begin{aligned} c_5 = &\frac{(p_2 - x/M)^{(1-\kappa)/\kappa}}{\kappa RC_{T1}M}\left(\frac{\alpha V_B}{1+\alpha} - \frac{\pi D^2\gamma}{4}x\right) \\ &+ \frac{\pi D^2\gamma(p_2 - x/M)^{1/\kappa}}{4RC_{T1}} \end{aligned} \tag{22}$$

$$c_6 = \frac{\pi D^2 \gamma p_2^{1/\kappa}}{4RC_{T2}} \tag{23}$$

B. Descent

Equations (1–7) of the climb model are also relevant to descent; all other equations must be modified. The pressure loss over the flow restrictions is reversed and the density is now calculated for atmospheric conditions

$$p_o - p_1 = \frac{\rho_o}{2} v_1^2 \xi_1 \tag{24}$$

$$p_o - p_2 = \frac{\rho_o}{2} v_2^2 \xi_2 \tag{25}$$

Here the pressure loss coefficients depend on the atmospheric conditions rather than on the conditions inside the instrument compartments as was the case during climb. Thus $\xi = \xi_0(p_0, T_0)$.

The continuity equations are also applied in the reversed direction using atmospheric density instead of the compartment densities

$$dm_1/dt = \rho_o \frac{\pi}{4} d_1^2 v_1 \tag{26}$$

$$dm_2/dt = \rho_o \frac{\pi}{4} d_2^2 v_2 \tag{27}$$

The energy equations are now written for adiabatic compression combined with the mixing of the inflowing air with air already in the compartments

$$\frac{dT_1}{dt} = \frac{\pi(\kappa T_0 - T_1)RT_1 d_1^2 v_1 \rho_0}{4p_1[\alpha V_B/(1+\alpha) - \pi D^2\gamma x/4]} \tag{28}$$

$$\frac{dT_2}{dt} = \frac{\pi(\kappa T_0 - T_2)RT_2 d_2^2 v_2 \rho_0}{4p_2[V_B/(1+\alpha) + \pi D^2\gamma x/4]} \tag{29}$$

As in the climb model, the atmospheric pressure change relative to the descending instrument must be known as a function of time $p_0 = f[h(t)]$. But here, because of the mixing in the charged compartments, also the atmospheric temperature $T_0 = g[h(t)]$ is required [for Eqs. (28) and (29)]. This set of simultaneous equations is now rearranged for the Runge-Kutta procedure. Here the functions c_i are defined in Eqs. (34–42).

$$\begin{aligned} \frac{dx}{dt} = &\left[c_{10} - \frac{R\rho_2}{p_2}(c_7 c_{11} - c_8 c_{11} c_{13}/c_{14} + c_9 c_{11})\right] \\ &\times\left[\frac{R\rho_2}{p_2} c_{11}(1/RM + c_8 c_{15}/c_{14}) + c_{13}\right]^{-1} = B \end{aligned} \tag{30}$$

$$\frac{dp_2}{dt} = R\left[c_9 + \frac{p_2}{R\rho_2 c_{11}}(c_{10} + c_{12}B)\right] \tag{31}$$

$$\frac{d\rho_1}{dt} = \frac{1}{c_8}\left(\frac{1}{R}\frac{dp_2}{dt} - \frac{B}{RM} - c_1\right) \tag{32}$$

$$\frac{d\rho_2}{dt} = \frac{1}{c_{11}}(c_{10} - c_{12}B) \tag{33}$$

As in the climb problem, $x(t)$ is the quantity of interest. But here, because of the more complex energy equations the densities ρ_1 and ρ_2 cannot be separated and therefore three auxiliary functions, p_2, ρ_1 and ρ_2 are necessary for the solution. The functions c_7 to c_{15} are defined as follows:

$$c_7 = \frac{\pi d_1^2\rho_0[\kappa T_0 - (p_2 - x/M)/R\rho_1][2(p_o - p_2 + x/M)/\rho_o\xi_1]^{1/2}}{4[\alpha V_B/(1+\alpha) - \pi D^2\gamma x/4]} \tag{34}$$

$$c_8 = (p_2 - x/M)R\rho_1 \tag{35}$$

$$c_9 = \frac{\pi d_2^2\rho_0[\kappa T_o - p_2/R\rho_2][2(p_0 - p_2)/\rho_0\xi_2]^{1/2}}{4[V_B/(1+\alpha) + \pi D^2\gamma x/4]} \tag{36}$$

$$c_{10} = \frac{\pi}{4}\rho_0 d_2^2(2(p_0 - p_2)/\rho_o\xi_2)^{1/2} \tag{37}$$

$$c_{11} = V_B/(1+\alpha) + (\pi/4)D^2\gamma x \tag{38}$$

$$c_{12} = (\pi/4)D^2\gamma\rho_2 \tag{39}$$

$$c_{13} = \frac{\pi}{4}d_1^2\rho_o\left(\frac{2(p_0 - p_2 + x/M)}{\rho_o\xi_1}\right)^{1/2} \tag{40}$$

$$c_{14} = \alpha V_B/(1+\alpha) - (\pi/4)D^2\gamma x \tag{41}$$

$$c_{15} = (\pi/4)D^2\gamma\rho_1 \tag{42}$$

Experiments

A model of a rate of climb indicator was built for the test rig. The model was designed to enable easy variations of the indicator parameters (compartments volume and flow restrictions) and to allow accurate measurements of the diaphragm displacements. The test rig is described schematically in Fig. 4. The rate of climb indicator RC is comprised of two compartments CM_1 and CM_2, their volumes can be varied by moving the pistons P. The interchangeable diaphragm has a small electric contact, D, at its center. This contact, when touching the tip of the micrometer MC closes the electric circuit comprising also the battery Ba and the bulb Bu. This circuit is used to calibrate the diaphragm and to evaluate the constant M. Each of the two compartments is equipped with a pressure transducer (PT_1 and PT_2). Their signal, after being conditioned in SC, is recorded by a multichannel uv recorder.

Each of the transducer compartments is connected to the container S which represents the varying environment. The pressure and temperature inside S can be controlled to create any desired initial temperature and pressure as well as any desired pressure variation $p_0(t)$. Rising pressure with time (relevant to descent) is created by charging S from a compressed air bottle C_1, through the two regulating valves R_1 (for course adjustment), and R_2 (for fine adjustment) and through the micrometric high precision valve V_3 used for final adjustment of $p_0(t)$. Falling pressure with time (relevant to climb) is created by evacuating the charged container S through the micrometric valve V_4 either directly into the atmosphere (when the valve V_6 is opened and V_5 is closed) or into a container C_2 held at constant negative gage pressure using the vacuum pump VP. Pressure vs time diagrams of S are recorded using the pressure transducer PT_3. This is done simultaneously with the recording of the signals from PT_1 and PT_2.

The compartments CM_1 and CM_2 are connected to S through two very fine adjustable micrometric valves V_1 and V_2. These two valves are designed to create a high pressure drop and represent the flow restrictions of the compartments. Adjustment of the valves causes variation of ξ_1 and ξ_2. The values of ξ_1 and ξ_2 can be measured using the rotameters Ro_1 and Ro_2.

The experiments were preceded by calibration of the diaphragm using the circuit MC-D-Ba-Bu. For a preset micrometer setting, the pressure difference required to close the contact was measured. The pressure difference was applied in both directions and it was found that the displacements in the pressure range applied are linear with negligible hysteresis. The value of M was $M = 1.79 \times 10^{-1}$ [m^3/kg]. The results are given in Fig. 5.

For each of the experiments ξ_1 and ξ_2 were set at the desired values and V_1 and V_2 adjusted. Further, the pressure function in S, $p_0(t)$, was fixed. The system was then brought to a steady initial condition and the transient process triggered using the solenoid valve SV_1 for descent experiments, or SV_2 for climb experiments. At each run the pressures detected by PT_1, PT_2, and PT_3 were simultaneously recorded.

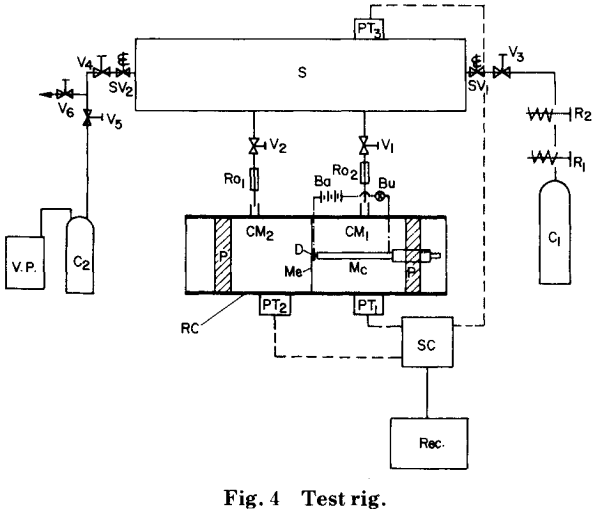

Fig. 4 Test rig.

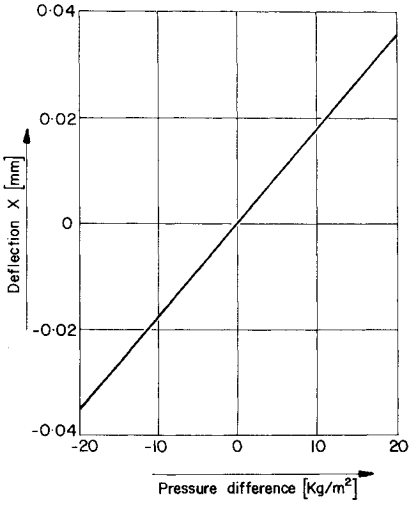

Fig. 5 Calibration line of the diaphragm.

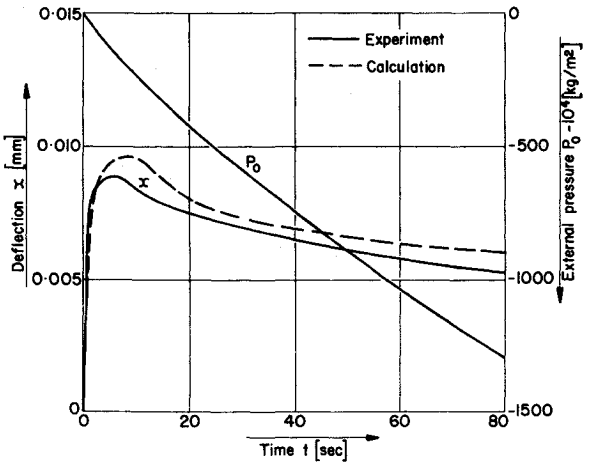

Fig. 6 Comparison of calculations and experiment for climb.

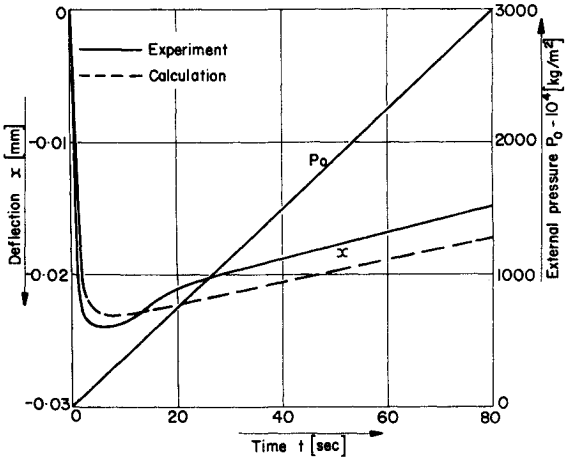

Fig. 7 Comparison of calculations and experiment for descent.

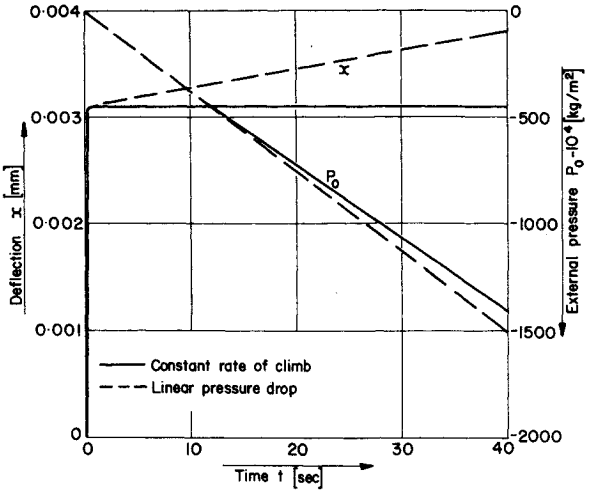

Fig. 8 Calculated deflection for constant rate of altitude variation and linear pressure change in the case of climb.

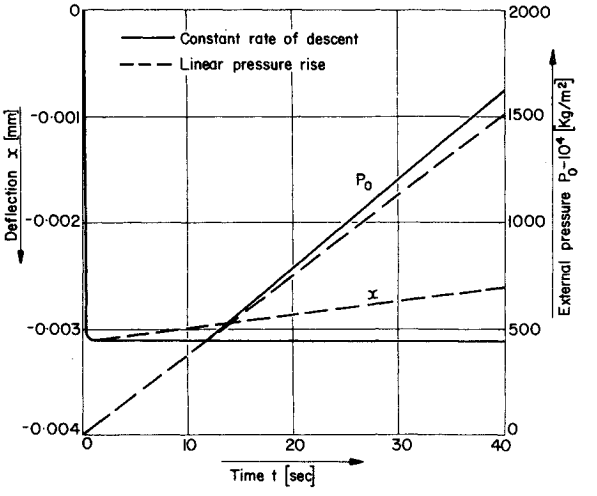

Fig. 9 Calculated deflection for constant rate of altitude variation and linear pressure change in the case of descent.

Figures 6 and 7 show the results of two typical runs for climb and descent, respectively. In each figure, the measured pressure curve in the container S is given. Also given are the measured and calculated displacement curves. The calculated curves represent numerical solutions of the mathematical model carried out with data of the experiment in question.

Discussion of the Results and Conclusions

The comparison between theory and experiment of Figs. 6 and 7 reveals acceptable agreement. The rate of the pressure change $|dp_0/dt|$, during the climb experiment was about half the rate of the pressure change of the descent experiment, resulting in smaller calculated and measured displacements. Also the nature of the external pressure change is different in both experiments. In the descent experiment the pressure function $p_0(t)$ was linear while during climb dp_0/dt was not constant, explaining the slightly different character of deflection curves. Both experiments do not represent constant rate of altitude variation being the result of arbitrary external pressure functions.

Figures 8 and 9 show the calculated results of a rate of climb indicator operating in an isothermal atmosphere. The curves are calculated for a constant rate of climb (Fig. 8) or constant rate of descent (Fig. 9) of 33m/sec in an atmosphere of 300°K. At these conditions the mathematical model produces a constant indication. The dashed lines in these figures give for comparison calculated results for linear external pressure variation.

Figures 6 and 7 demonstrate that the mathematical model can produce results which represent reality to an aggreeable accuracy, varifying the model quantitatively. Figures 8 and 9 show that the mathematical model produces a constant indication at constant rate of altitude variation. Further, in Fig. 8, dp_0/dt of the constant climb curve is always smaller than dp_0/dt of the linear presure line. This explains the smaller indication for constant rate of climb in Fig. 8. The opposite situation is observed in Fig. 8 for descent. Here dp_0/dt of the constant descent curve is always larger than the constant rate of pressure change of the linear pressure rise. Consequently, the indications for constant descent are larger than the indications for linear pressure rise. The results of Figs. 8 and 9 varify the mathematical model quantitatively.

Thus, it can be concluded that the mathematical model presented here can be used with agreeable confidence as a tool for the design of rate of climb indicators, as well as a basis for optimization or simulation programs.

References

[1]Bestelmeyer, A., "Zur Theorie des Ballonvariometers," *Physikalische Zeitschrift*, Vol. 11, 1910, pp. 763–768.

[2]Mears, A. H., "Statoscopes and Rate of Climb Indicators," Rept. 126, 1922, NACA.

[3]Eaton, H. N., *Aircraft Instruments*, Ronald Press, New York, 1926, pp. 46–52.

[4]Stewart, C. J., *Aircraft Instruments*. Wiley, New York, 1930, pp. 42–51.

[5]McKay, W., "Dynamic Characteristics of Pressure Operated Aircraft Instruments," Ph.D. thesis, 1935, MIT, Cambridge, Mass.

[6]Oppelt, W. and Wenk, F., "Theoretische Betrachtung des Luftdruckvariometers und Richteinien fur Entwurf and Prufung," *Luftfahrtforschung*, Vol. 14, pp. 537–541, (1937).

[7]Draper, C. S. and Schliestett, G. V., "Dynamic Errors of the Rate of Climb Meter," *Journal of the Aerospace Sciences*, Vol. 5, 1938, pp. 426–430.

[8]Johnson, D. P., "Aircraft Rate of Climb Indicators," TR 666, 1939, NACA.

[9]DeJuhasz, K. J., "Graphical Analysis of Response Characteristics of Rate of Climb Indicators," *Journal of the Aerospace Sciences*, Vol. 11, 1944, pp. 48–54.

[10]Takeda, S., "Theoretical and Experimental Investigation of Rate of Climb Indicators," Rept., Dec. 1957, Technical College of Hosei University, Tokyo, Japan.

[11]Considire, D. M., *Process Instruments and Controls*, McGraw-Hill, New York, 1957.

[12]Andreeva, L. E., *Elastic Elements of Instruments*, Israel Program for Scientific Translations, 1966.

AUGUST 1974 J. AIRCRAFT VOL. 11, NO. 8

In-Flight Oxygen Generation for Aircraft Breathing Systems

Edward J. Boscola
Naval Air Development Center, Warminster, Pa.

Operational and logistics problems associated with liquid oxygen (LOX) breathing supply systems have shown the need for developing methods of generating oxygen directly on board the aircraft for aircrew breathing. Concepts presently being developed are based upon fluomine chemical sorbent and electrochemical concentrator processes. The fluomine process is a temperature cycled chemical system using the fluomine for reversibly sorbing oxygen from engine bleed air. The electrochemical process uses a combination fuel cell and electrolysis cell reaction to generate oxygen. Oxygen from an air stream is reduced on the cathode to form water, the water is then electrolyzed at the anode to evolve pure gaseous oxygen. With the aid of necessary aircraft resources (electrical power, air, heating, and cooling), these techniques extract oxygen directly from engine bleed air during all flight operations. The oxygen generation systems produce oxygen at approximately 99.5% purity and is sufficient to meet the breathing requirements of two men during all in-flight operations. Ground and aircraft carrier support will be eliminated or minimized to improve efficiency and safety of flight operations. Aircraft turn around time with respect to oxygen will be reduced to nearly zero while maintenance periods will have a minimum time of 1000 flying hr.

Introduction

OPERATIONAL limitations imposed as a result of the current method of handling and stowing liquid oxygen (LOX) supply systems often restrict the availability of aircraft for extended missions. In addition, logistics and maintenance problems, dangers of fire, and contamination associated with LOX pose a continued threat to the effectiveness of the total aircraft weapons system.

The limitations and problems associated with LOX become increasingly severe both to carrier-based aircraft and to aircraft operating from advanced sea and ground bases as the performance of tactical aircraft is developed to meet extended operational and mission requirements. The cost of the LOX generating capacity of an aircraft carrier, both in dollars and in carrier space and electrical power output, is prohibitive as are the logistics problems with transporting LOX to the carrier from a shore based source of supply.

To eliminate the problems associated with LOX, new forms of oxygen generation methods which produce oxygen directly on board aircraft are presently being developed under a joint Navy/Air Force effort. Navy interest in new oxygen generation techniques is directed primarily toward carrier-launched and retrieved fighter/attack aircraft. However, the equipment can be equally applicable to all fixed-wing and rotary-wing aircraft that require breathing oxygen for the aircrew.

Design Criteria

The basic requirements for oxygen generating systems are shown in Table 1. With the necessary aircraft resources the systems shall generate oxygen at approximately 99.5% purity at a rate sufficient to meet the breathing requirements of two men during all in-flight operations, in addition to start-up and taxiing conditions and underwater emergencies. The maximum electrical power to support the system is 7 kva. The system is intended to replace the current stored LOX system and, thereby, eliminate or minimize ground and aircraft carrier support, improve efficiency and safety of flight operations, and to have a minimum time of 1000 flying hr between maintenance periods. Flight time between servicing is 15 hr and in order to satisfy quick turn-around time requirements, servicing shall not take more than 5 min per aircraft.

Presented as Paper 73-1348 at the AIAA Crew Equipment Systems Conference, Las Vegas, Nev., November 1-9, 1973; submitted December 6, 1973; revision received May 7, 1974.

Index category: Aircraft Cabin Environment and Life Support Systems.

*Program Manager, Crew Systems Department.